NANO LETTERS

Letter

pubs.acs.org/NanoLett

A New Twist on Scanning Thermal Microscopy

Michael E. McConney,*[,†,‡] Dhaval D. Kulkarni,[‡] Hao Jiang,[†] Timothy J. Bunning,[†] and Vladimir V. Tsukruk[‡]

[†]Materials and Manufacturing Directorate, Air Force Research Laboratory, WPAFB, Ohio 45433, United States

[‡]School of Materials Science and Engineering, Georgia Institute of Technology, Atlanta, Georgia 30332, United States

Supporting Information

ABSTRACT: The thermal bimorph is a very popular thermal sensing mechanism used in various applications from meat thermometers to uncooled infrared cameras. While thermal bimorphs have remained promising for scanning thermal microscopy, unfortunately the bending of the bimorph directly interferes with the bending associated with topographical information. We circumvent this issue by creating bimorphs that twist instead of bending and demonstrate the superior properties of this approach as compared to conventional scanning thermal microscopy.

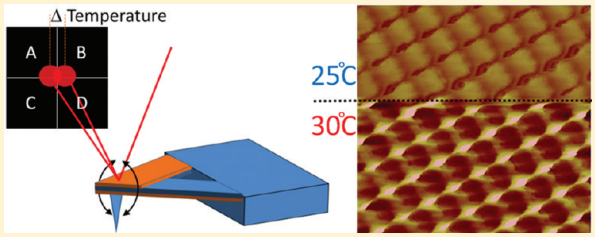

KEYWORDS: *Scanning thermal microscopy, scanning thermal twisting microscopy, thermal transport, nanoscale thermometry, thermal bimorph*

Scanning thermal microscopy (SThM) is a critical technique in the analysis of thermal, electronic, and photonic transport at dimensions approaching the mean free path of phonons and other quasi particles.[1,2] Unfortunately, commercial probes are typically limited to submicrometer spatial resolution and thermal sensitivity of a fraction of a degree.[3−5] Over the years, many different thermal sensing mechanisms have been explored for SThM including the Seebeck effect,[6−10] temperature dependent resistance,[11] and thermal bimorph bending.[12] The thermal bimorph mechanism utilizes the difference in thermal expansion of two materials intimately bound to cause bending stresses in response to heat.[13] Thermal bimorph bending has very promising properties but has remained impractical for SThM because the thermal bending directly interferes with topography imaging. Here, we re-examine the bimorph mechanism for SThM and address this major limitation by introducing scanning thermal twisting microscopy. The thermal-topographical signal interference issue is solved by creating a probe with an asymmetrical bimorph geometry that twists, instead of bends, in response to heat.

Since the introduction of thermal probes,[14] there have been major improvements in SThM, but the widespread use has unfortunately been hindered by the high cost of commercial probes, as well as their modest spatial (typically ∼100 nm) and thermal resolution (∼0.1 K).[15−20] Furthermore, commercial resistive-based probes can also suffer from cross-talk between thermal and electrical signals when imaging electrical circuits. Thermal bimorphs do not suffer from these setbacks. In fact, thermal bimorphs transduced with an atomic force microscopy (AFM) quadrant photodetector have a theoretical limit of thermal resolution on the order of 10^{-5} K, 2 orders of magnitude better than the theoretical limit of electrical techniques.[12] As mentioned, the impediment to this approach is that the thermal signal and the topographical signal utilize the same signal transduction channel, namely normal deflection of the laser spot in the quadrant photodiode (Figure 1a). In order for SThM to function properly, the tip−surface distance must be accounted for by performing SThM in conjunction with AFM. The topography imaging of the AFM is critical to maintaining the thermal probe/sample distance, thereby enabling the inherent thermal properties to be mapped. Therefore, typically the thermal bimorph effect is considered a nuisance despite promising properties. While the thermal bimorph effect interferes with the topographical signal, this has not stopped researchers from trying to utilize this transduction mechanism for SThM. For instance, in order to circumvent the signal overlap issue, Majumdar and co-workers used a microfabricated resistive heating substrate to sinusoidally heat the sample at a frequency on the order of 100 Hz.[12] While this technique worked fairly well, it unfortunately requires a microfabricated substrate and complicated electronics and therefore did little to address cost issues associated with SThM.

Scanning thermal twisting microscopy (STTM) addresses the thermal-topographical signal interference issue by creating an asymmetrical bimorph geometry that twists the microfabricated cantilever with thermal changes, thereby using the lateral deflection signal ((A + C) − (B + D)) for thermal imaging, while maintaining the normal deflection signal ((A + B) − (C + D)) for concurrent topographical imaging (Figure 1b). This design does not require complicated and expensive electronic equipment; instead the imaging technique relies only on the hardware already typically provided by AFM manufacturers.

Inherently, the lateral (twisting) spring constants of cantilevers are much higher than the normal spring constants. V-shaped cantilevers have lateral (twisting) spring constants

Received: October 7, 2011
Revised: January 18, 2012
Published: January 25, 2012

Report Documentation Page

Form Approved
OMB No. 0704-0188

1. REPORT DATE	2. REPORT TYPE	3. DATES COVERED
25 JAN 2012		**00-00-2012 to 00-00-2012**

4. TITLE AND SUBTITLE	5a. CONTRACT NUMBER
A New Twist on Scanning Thermal Microscopy	5b. GRANT NUMBER
	5c. PROGRAM ELEMENT NUMBER
6. AUTHOR(S)	5d. PROJECT NUMBER
	5e. TASK NUMBER
	5f. WORK UNIT NUMBER
7. PERFORMING ORGANIZATION NAME(S) AND ADDRESS(ES) **Air Force Research Laboratory,Materials and Manufacturing Directorate,Wright Patterson AFB,OH,45433**	8. PERFORMING ORGANIZATION REPORT NUMBER
9. SPONSORING/MONITORING AGENCY NAME(S) AND ADDRESS(ES)	10. SPONSOR/MONITOR'S ACRONYM(S)
	11. SPONSOR/MONITOR'S REPORT NUMBER(S)

12. DISTRIBUTION/AVAILABILITY STATEMENT
Approved for public release; distribution unlimited

13. SUPPLEMENTARY NOTES

14. ABSTRACT

The thermal bimorph is a very popular thermal sensing mechanism used in various applications from meat thermometers to uncooled infrared cameras. While thermal bimorphs have remained promising for scanning thermal microscopy, unfortunately the bending of the bimorph directly interferes with the bending associated with topographical information. We circumvent this issue by creating bimorphs that twist instead of bending and demonstrate the superior properties of this approach as compared to conventional scanning thermal microscopy.

15. SUBJECT TERMS

16. SECURITY CLASSIFICATION OF:			17. LIMITATION OF ABSTRACT	18. NUMBER OF PAGES	19a. NAME OF RESPONSIBLE PERSON
a. REPORT	b. ABSTRACT	c. THIS PAGE			
unclassified	**unclassified**	**unclassified**	**Same as Report (SAR)**	**6**	

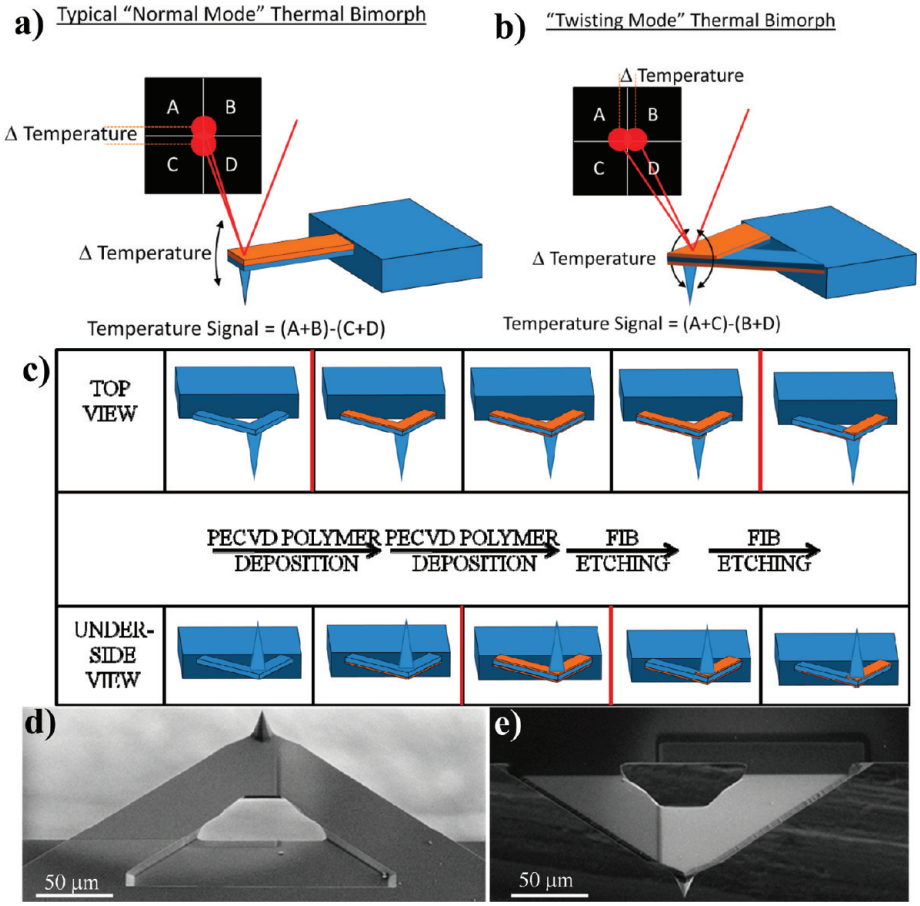

Figure 1. (a) A schematic of the bending motion of a typical thermal bimorph. The bimorph bending signal channel is the difference between the top two photodetectors and the bottom two photodetectors, which is the same as the topographical signal channel. (b) A schematic of the twisting motion of a thermal twisting bimorph. The bimorph twisting signal channel is the difference between the left two photodetectors and the right two photodetectors, which is different than the topographical signal channel. (c) A schematic indicating the fabrication process used for making V-shaped thermal twisting probes. (d) Tipside-oriented and (e) backside-oriented scanning electron micrographs of a STTM probe.

that are roughly 500 times more stiff than normal bending spring constants.[21] Therefore, to realize thermal twisting probes it is critical to maximize the thermal expansion mismatch between the materials to overcome the inherently high lateral stiffness. Most thermal bimorph work thus far has involved ceramic/metal composites with rather poor sensitivity due to a small thermal expansion difference of the two materials making up the bimorph. Instead, polymer/ceramic composites have proven to be much more sensitive due to high thermal expansion coefficient of the polymeric materials.[22] LeMieux et al. developed highly sensitive probes through the use of plasma polymer–silicon bimorphs with high mismatch of thermal properties.[23−25] These cantilevers had an unprecedented thermal resolution of 0.2 mK. Furthermore, this work demonstrated plasma polymers have excellent adhesion to silicon and excellent long-term stability.

The thermal twisting probes presented here are fabricated by first depositing plasma polymerized film on both sides of commercially available V-shaped "tapping" cantilever ($f \approx 330$ kHz, $k_N \approx 48$ N/m) as schematically shown in Figure 1c. Half of the top-side coating is then removed via focused ion beam (FIB) milling, followed by removing the opposite half of the bottom-side coating (Figure 1c). This procedure leaves each leg of the v-shaped cantilever as a thermal bimorph but with opposite orientations. The combined thermal actuation is a twisting motion, instead of the typical normal bending, as is depicted in Figure 1b. Scanning electron micrographs of a twisting bimorph cantilever are presented in Figure 1d,e.

Finite element modeling was used to explore the deformation of the twisting bimorph and the sensitivity dependence on the laser spot position with respect to the cantilever surface (Figure 2). The modeling of thermal bending V-shaped twisting cantilevers indicated that the cantilevers would provide the highest thermal lateral sensitivity $[(\partial/\partial T)(\partial x/\partial z)]$ when the laser spot was positioned near the center of the cantilever in the $x-y$ plane (refer to Figure 2). Furthermore, in that center region, the thermal normal bending sensitivity $[(\partial/\partial T)(\partial x/\partial z)]$ would ideally be zero, thereby preventing interference with the topographical signal. On either side (offset in the x-axis) of the center point are saddle points (bright red and bright blue regions in Figure 2), which are regions where the cantilever is parallel with the horizon and thus are completely insensitive to thermal signal. Adjacent to these saddle points along the y-axis are regions of enhanced normal bending sensitivity $[(\partial/\partial T)(\partial x/\partial z)]$ and thus increased interference with the topographical signal. Therefore, it should be clear that positioning of the laser spot is critical to maximizing the lateral thermal sensitivity and minimizing the normal thermal sensitivity. Fortunately, centering the laser spot is a relatively simple and routine procedure with the use of an optical microscope associated with most AFMs.

dx.doi.org/10.1021/nl203531f | Nano Lett. 2012, 12, 1218–1223

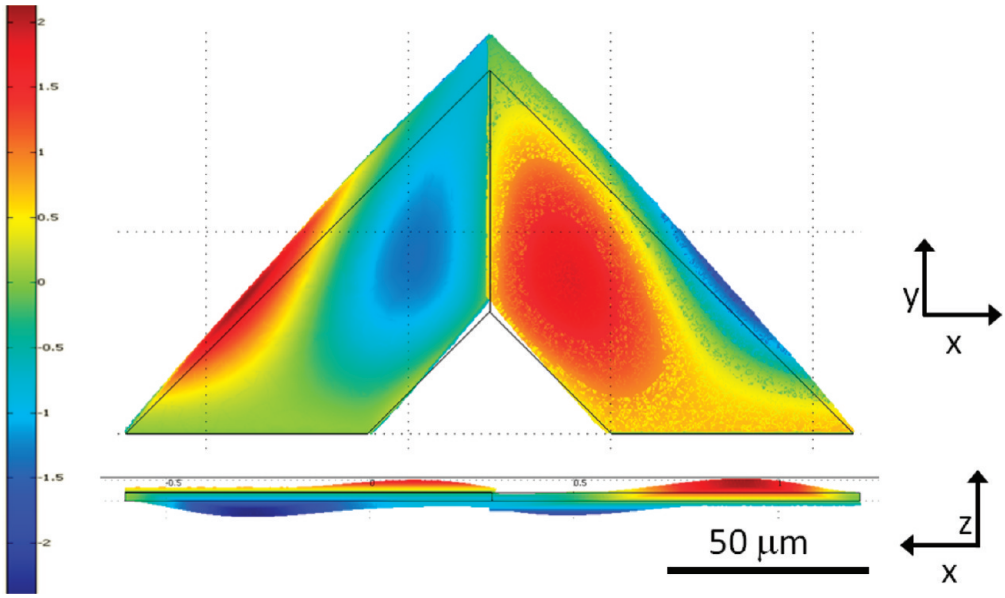

Figure 2. The result of modeling the thermal response of the twisting bimorph cantilever geometry shown from two different perspectives. The *z*-displacement color scale has units of nanometers.

The thermal sensitivity of normal and lateral bending was quantified by suspending the cantilever above a thermal-electric cooler/heater with a tip−surface distance of roughly 20 μm, as estimated by Z-stepper motor movement. The temperature was incrementally changed, while monitoring the normal and lateral photodiode signals. Figure 3 shows a plot of lateral and normal

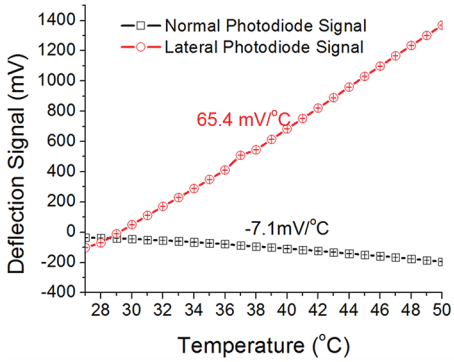

Figure 3. A plot of lateral and normal deflection of a representative twisting bimorph cantilever versus surrounding temperature.

photodiode signal versus temperature. The lateral thermal sensitivity was measured to be 65.4 mV/K, whereas the absolute normal thermal sensitivity was measured to be 7.1 mV/K, almost an order of magnitude less. The lateral signal noise was measured to be 1.8 mV, thereby leading to a noise-limited thermal resolution of 27 mK, which is manifold better than thermal resolution of the traditional mode (0.11K as estimated for the same tip).

The STTM images presented here were obtained in "lift mode" to definitively show that frictional forces do not play a part in creation of the thermal image and to reduce the capillary bridge. Lift mode is a common noncontact scanning method used in several scanning probe imaging techniques including magnetic force microscopy and electrostatic force microscopy.[26] Furthermore, lift-mode has also recently been used in a calibration approach to account for environmental thermal losses in order obtain quantitative SThM images.[27] The images presented here were acquired by recording surface topography in the first pass of the probe and the lateral thermal signal was obtained while retracing the topography profile with a set lift height above the surface. Lift-mode maintains a constant tip−surface distance, which minimizes surface damage and lateral friction forces that interfere with the thermal signal. As the temperature was raised, the maximum stable lift height decreased. This behavior indicates that the predominant thermal conduction mechanism is a water bridge between the surface and the tip, which is typical of SThM performed at atmospheric conditions.[28] Thermal images were not significantly affected by scanning speeds as high as 2 Hz with a resolution of 512 points per line, indicating that the thermal equilibration time is on the order of milliseconds. While lift-mode essentially eliminates frictional contributions, imaging was also performed at different scanning angles to confirm that frictional forces were not contributing to the thermal image.

To further demonstrate that the lateral deflection signal is in fact imaging thermal properties and the normal deflection signal is imaging topography independent of one another, the sample temperature was changed from heating to cooling (with respect to room temperature) in the middle of the imaging, expecting to see a contrast inversion in the lateral deflection image and no change in the topographical image. The results of this so-called "litmus test" on a rough surface serve as a strong indicator of the characteristics of the system. The contrast inversion in the lateral image is expected because the absolute magnitude of the image contrast is directly related to the thermal conductivity of the sample. As shown in Figure 1, the lateral signal is comprised of the output from the left photodetectors minus the output of the right photodetectors ((A + C) − (B + C)). In this case the cantilever twists to the left upon heating, creating a lighter image contrast. Thus in the sample heating regime, regions with higher thermal conductivity will appear lighter than regions with lower conductivity because the tip is being heated more in the higher thermal conductivity regions. Whereas in the sample cooling regime, regions with higher thermal conductivity will appear darker than regions with lower conductivity because

dx.doi.org/10.1021/nl203531f | *Nano Lett.* 2012, 12, 1218−1223

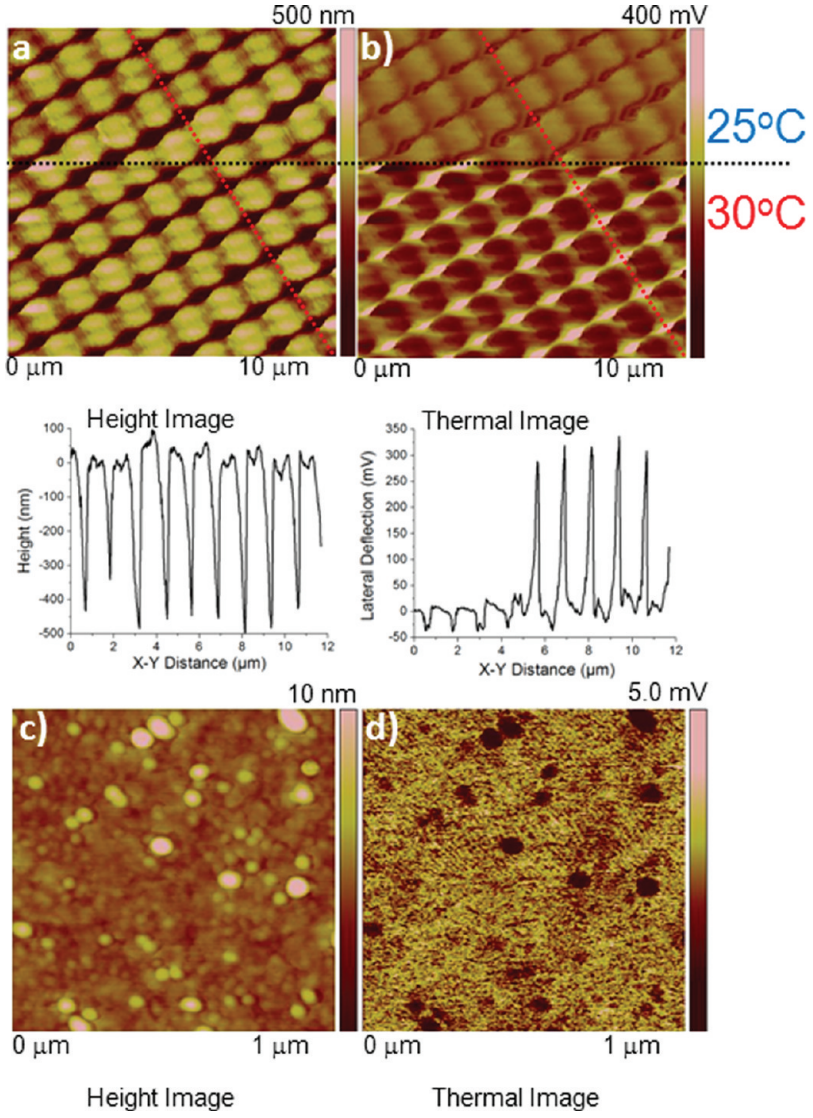

Figure 4. (a) The height image and (b) the lateral deflection thermal image of patterned SU-8 with respective slice plots. The temperature was changed from 25 to 30 °C half way through the acquisition of the images. The black dotted line indicates the location at which the temperature was changed. The red dotted lines indicate the location that the respective slice plots are from. (c) The height image and (d) the lateral deflection thermal image of gold nanoparticles taken at 26 °C. The thermal images in (b) and (d) were captured with lift heights of 50 and 10 nm, respectively.

more heat is being drawn from the tip in the higher thermal conductivity regions.

The images resulting from this litmus test, taken from a sample patterned with interference lithography (SU-8 at 1.25 μm periodicity), are shown in Figure 4a,b. The tip/sample thermal conductivity is much higher in the sample depressions because the tip−sample contact area is much higher and because the glass substrate has a higher thermal conductivity than the SU-8 photoresist. It is evident that the height image (Figure 4a) does not change considerably upon changing from heating to cooling, whereas the contrast inverts in the lateral deflection image (Figure 4b) after the temperature change.

The spatial resolution of thermal microscopy was quantified from the STTM images using the following equation

$$\Delta x = \frac{\Delta T_{\mathrm{n}}}{\left(\frac{\mathrm{d}T_{\mathrm{t}}}{\mathrm{d}x}\right)_{\max}}$$

where ΔT_n is the noise of the temperature signal and $(\mathrm{d}T_t/\mathrm{d}x)_{max}$ is defined as the largest temperature gradient signal measured.[2,28] STTM images of interference lithography samples show a max thermal signal gradient of 2977 mV/μm and the noise of 1.8 mV leading to a spatial resolution of 0.61 nm, which is about 2 orders of magnitude better than that of conventional SThM. Therefore, STTM spatial resolution is limited by the radius of curvature of the tip and not the thermal sensitivity of the cantilever. In order to confirm the lateral spatial resolution of the thermal imaging a standard gold nanoparticle sample (5 nm radius) was imaged (Figure 4c,d) at 26 °C. The lateral feature sizes of the topographical image and the thermal image are essentially identical indicating a modest and similar tip dilation effect. Therefore, the spatial resolution of the thermal imaging is in fact limited by the tip radius which can be as low as 5 nm for microfabricated tips.

In conclusion, scanning thermal twisiting microscopy is a novel method of mapping nanoscale thermal properties using a twisting asymmetrical bimorph cantilever. This twisting motion

dx.doi.org/10.1021/nl203531f | Nano Lett. 2012, 12, 1218–1223

allows the thermal signal to be isolated from the normal deflection caused by surface topography thus facilitating nanoscale spatial resolution and milliKelvin (mK) thermal resolution. STTM simplifies thermal imaging with significant improvement of the spatial and thermal resolution. STTM flourishes near room temperature, thereby making it highly promising for biological imaging applications, mapping of electric microdevices, and electromechanical systems. STTM does not use electronics for signal transduction and therefore does not suffer from the same current leakage issues as other methods, making it ideal to study thermal and electronic transport simultaneously. The fabrication of the miniature asymmetrical bimorph cantilevers is simple and therefore stands as a possible mass-production of cheap and highly sensitive thermal imaging probes with nanoscale spatial resolution and mK thermal resolution not existing now.

Experimental Section. *Probe Fabrication and STTM.* Mikromasch NSC-11 (Al-BS) probes were coated with a 90 nm thick plasma polyacrylonitrile films on the top side and underside of the probe. The plasma-enhanced chemical vapor deposition was done in a custom PECVD chamber.[23] Argon was used as a plasma carrier gas, which entered the chamber 20 cm upstream of the plasma generation zone at a flow rate of 20 cc/min. The plasma was generated with a capacitive coupled radio frequency discharge source with a frequency of 13.56 MHz and a power of 20 W. The acrylonitrile monomer vapor entered the chamber approximately 10 cm downstream of the plasma source at a flow rate of 1 cc/min. The cantilever chips (Mikromasch NSC-11 Al-BS) were mounted on a silicon wafer substrate that was mounted to the chamber chuck about 3 cm downstream from the monomer inlet stream. Plasma polyacrylonitrile films (90 nm thick) were deposited on the each side of the probe in two separate identical deposition runs. The thickness was measured by ellipsometry on the silicon wafers. Focused ion beam milling (FEI DB-235) was used to remove opposing halves of the two polymer coatings. Typically, the polymer film was removed by raster scanning the FIB at an accelerating voltage of 30 kV and a current of 20 nA over a 130 × 115 μm rectangular area that included the polymer region targeted for removal for 3 min. Most of the STTM work (including the images presented in Figure 4) was performed with a DI-3000 equipped with a Nanoscope IV controller (Veeco) but some was also performed with a DI3100 with a Nanoscope V controller. The sample temperature was controlled with 2510 TEC controller (Keithley) connected to a thermoelectric cooler with a surface-mounted thermistor. Further details regarding the imaging procedure are presented in the Supporting Information.

Simulation. Finite element analysis (FEA) using COMSOL Multiphysics 3.2 software with a structural mechanics module has been used to understand the deflection of the cantilever in response to changes in temperature. The FEA modeling involves minimizing the energy of the individual mesh elements. The bimaterial structure was meshed into over 40 000 elements. The silicon cantilever modeled with the same dimensions as the Mikromasch NSC-11 cantilevers used in the study. The NSC-11 cantilevers have a thickness of 2 μm, a length (chip edge to tip of V) of 90 μm, and an arm width of 40 μm. The material parameters for the cantilever were obtained from COMSOL as default values for silicon. The plasma polyacrylonitrile material properties were taken from previous work (see refs 21 and 22.). A modulus of 2 GPa, an absolute thermal expansion of 3.1×10^{-4}, and a Poisson's ratio of 0.4 was used. The modeled thermal bending data presented in Figure 2 was produced by change the temperature from 20 to 30 °C.The output of the modeling process is a color map of cantilever defection that was used to understand the normal and lateral bending with the changes in temperature.

■ ASSOCIATED CONTENT

Supporting Information

Additional information and figures. This material is available free of charge via the Internet at http://pubs.acs.org.

■ AUTHOR INFORMATION

Corresponding Author

*E-mail: michael.mcconney@wpafb.af.mil.

Notes

The authors declare the following competing financial interest(s):MEM has submitted a provisional patent application regarding this work.

■ ACKNOWLEDGMENTS

The authors would like to thank Rachel Jakubiak, Shane Juhl, Scott Apt, David Tomlin, Vincent Tondiglia, Lirong Sun, Maneesh Gupta, Abigail Juhl, and Michael Birnkrant for their help. We would also like to thank Professor Srikanth Singamaneni and Kyle Anderson for useful discussions. M.M. recognizes the support of the National Research Council Research Associate Program at Air Force Research Laboratory throughout this work. The work at Georgia Tech was supported by the Semiconductor Research Corporation (GRC Grant 2008OJ1864.1281) and Air Force Office of Scientific Research (Grant FA9550-08-1-0446 and FA9550-09-1-0162).

■ REFERENCES

(1) Gmelin, E.; Fischer, R.; Stitzinger, R. *Thermochim. Acta* **1998**, *310* (1−2), 1−17.
(2) Shi, L.; Majumdar, A. *Microscale Thermophys. Eng.* **2001**, *5* (4), 251−265.
(3) *Thermal Analysis of Polymers*; Menczel, J. D.; Prime, R. B., Eds.; John Wiley & Sons, Inc.: New York, 2008.
(4) Gorbunov, V. V.; Fuchigami, N.; Hazel, J. L.; Tsukruk, V. V. *Langmuir* **1999**, *15* (24), 8340−8343.
(5) Tsukruk, V. V.; Gorbunov, V. V.; Fuchigami, N. *Thermochim. Acta* **2002**, *395* (1−2), 151−158.
(6) Majumdar, A.; Carrejo, J. P.; Lai, J. *Appl. Phys. Lett.* **1993**, *62* (20), 2501−2503.
(7) Shi, L.; Kwon, O.; Miner, A. C.; Majumdar, A. *J. Microelectromech. Syst.* **2001**, *10* (3), 370−378.
(8) Shi, L.; Majumdar, A. *J. Heat Transfer* **2002**, *124* (2), 329−337.
(9) Pollock, H. M.; Hammiche, A.; Song, M.; Hourston, D. J.; Reading, M. *J. Adhes.* **1998**, *67* (1−4), 217−234.
(10) Patrick, C. F.; Byeonghee, L.; William, P. K. *Nanotechnology* **2012**, *23* (3), 035401.
(11) Pylkki, R. J.; Moyer, P. J.; West, P. E. *Jpn. J. Appl. Phys.* **1994**, *33*, 3785−3790.
(12) Nakabeppu, O.; Chandrachood, M.; Wu, Y.; Lai, J.; Majumdar, A. *Appl. Phys. Lett.* **1995**, *66* (6), 694−696.
(13) Singamaneni, S.; LeMieux, M. C.; Lang, H. P.; Gerber, C.; Lam, Y.; Zauscher, S.; Datskos, P. G.; Lavrik, N. V.; Jiang, H.; Naik, R. R.; Bunning, T. J.; Tsukruk, V. V. *Adv. Mater.* **2008**, *20* (4), 653−680.
(14) Williams, C. C.; Wickramasinghe, H. K. *Appl. Phys. Lett.* **1986**, *49* (23), 1587−1589.
(15) Majumdar, A. *Annu. Rev. Mater. Sci.* **1999**, *29* (1), 505−585.
(16) Pollock, H. M.; Hammiche, A. *J. Phys. D: Appl. Phys.* **2001**, *34* (9), R23.

(17) McConney, M. E.; Singamaneni, S.; Tsukruk, V. V. *Polym. Rev.* **2010**, *50* (3), 235−286.
(18) Hammiche, A.; Pollock, H. M.; Song, M.; Hourston, D. J. *Meas. Sci. Technol.* **1996**, *7* (2), 142.
(19) Reading, M. *Trends Polym. Sci.* **1993**, *1*, 248−253.
(20) Hinz, M.; Marti, O.; Gotsmann, B.; Lantz, M. A.; Durig, U. *Appl. Phys. Lett.* **2008**, *92* (4), 043122−3.
(21) Hazel, J. L.; Tsukruk, V. V. *J. Tribol.* **1998**, *120* (4), 814−819.
(22) Lin, Y. H.; McConney, M. E.; LeMieux, M. C.; Peleshanko, S.; Jiang, C.; Singamaneni, S.; Tsukruk, V. V. *Adv. Mater.* **2006**, *18* (9), 1157−1161.
(23) LeMieux, M. C.; McConney, M. E.; Lin, Y. H.; Singamaneni, S.; Jiang, H.; Bunning, T. J.; Tsukruk, V. V. *Nano Lett.* **2006**, *6* (4), 730−734.
(24) Singamaneni, S.; Le Mieux, M. C.; Jiang, H.; Bunning, T. J.; Tsukruk, V. V. *Chem. Mater.* **2007**, *19* (2), 129−131.
(25) Singamaneni, S.; McConney, M. E.; LeMieux, M. C.; Jiang, H.; Enlow, J. O.; Bunning, T. J.; Naik, R. R.; Tsukruk, V. V. *Adv. Mater.* **2007**, *19* (23), 4248−4255.
(26) Tsukruk, V. V.; Singamaneni, S. *Scanning Probe Microscopy of Soft Matter: Fundamentals and Practices*; Wiley-VCH: New York, 2012.
(27) Kim, K.; Chung, J.; Hwang, G.; Kwon, O.; Lee, J. S. *ACS Nano* **2011**, *5* (11), 8700−8709.
(28) Luo, K.; Shi, Z.; Varesi, J.; Majumdar, A. *J. Vac. Sci. Technol., B* **1997**, *15* (2), 349−360.

dx.doi.org/10.1021/nl203531f | *Nano Lett.* 2012, 12, 1218−1223